Geophysical Prospecting

EAGE EUROPEAN ASSOCIATION OF GEOSCIENTISTS & ENGINEERS

Geophysical Prospecting, 2015, **63**, 271–282 doi: 10.1111/1365-2478.12189

Anisotropy signature in reverse-time migration extended images

Paul Sava[1]* and Tariq Alkhalifah[2]

[1]*Colorado School of Mines, Golden, CO 80401 USA, and* [2]*King Abdullah University of Science and Technology, Thuwal 23955-6900, Saudi Arabia*

Received July 2013, revision accepted March 2014

ABSTRACT

Reverse-time migration can accurately image complex geologic structures in anisotropic media. Extended images at selected locations in the Earth, i.e., at common-image-point gathers, carry rich information to characterize the angle-dependent illumination and to provide measurements for migration velocity analysis. However, characterizing the anisotropy influence on such extended images is a challenge. Extended common-image-point gathers are cheap to evaluate since they sample the image at sparse locations indicated by the presence of strong reflectors. Such gathers are also sensitive to velocity error that manifests itself through moveout as a function of space and time lags. Furthermore, inaccurate anisotropy leaves a distinctive signature in common-image-point gathers, which can be used to evaluate anisotropy through techniques similar to the ones used in conventional wavefield tomography. It specifically admits a V-shaped residual moveout with the slope of the "V" flanks depending on the anisotropic parameter η regardless of the complexity of the velocity model. It reflects the fourth-order nature of the anisotropy influence on moveout as it manifests itself in this distinct signature in extended images after handling the velocity properly in the imaging process. Synthetic and real data observations support this assertion.

INTRODUCTION

Wave-equation depth migration is powerful and accurate for imaging complex geology, but its potential can only be achieved with high-quality models of the Earth (Gray *et al.* 2001). Moreover, even if a good-quality Earth model is known, accurate imaging requires a wave propagation engine capable of placing information recorded on the surface at accurate positions in the subsurface. Imaging using reverse-time migration (RTM) (Baysal, Kosloff, and Sherwood 1983; McMechan 1983), addresses this challenge, although this technique is still fairly computationally intensive, especially in anisotropic media.

Imaging with RTM can be described as a sequence of two main steps. The first step consists of wavefield reconstruction from known quantities on the surface, i.e., the wavelet known at the source position and the data known at the receiver positions. The wavefields are reconstructed everywhere in the medium as a solution of the wave equation. This reconstruction makes use of an Earth model that can be, for example, anisotropic. The second step represents an imaging condition, i.e., a procedure that identifies places in the subsurface where the reconstructed wavefields coincide. The imaging condition is often implemented by cross-correlation of the wavefields. A general imaging condition preserves in the output the space and time correlation lags, and thus, it can be named an extended imaging condition of which the conventional cross-correlation is a special case.

Assuming that the wavefields are accurately reconstructed in the subsurface, the correlation maximizes at zero lag, both in space and in time. Accurate reconstruction implies not only that we use a correct earth model but also that the recorded data completely illuminate the subsurface in the area under investigation. Good illumination requires that we collect data with wide azimuth and long offsets and that the geologic structure does not obstruct our imaging target

*E-mail: psava@mines.edu

© 2014 European Association of Geoscientists & Engineers

inside the Earth through, for example, illumination caused by salt bodies.

Typically, the problem of large extended image output can be addressed by analyzing subsets of the image. We can consider common image gathers (CIGs), which are subsets of extended images constructed for various lags at fixed horizontal coordinates in the Earth. For example, we can use space-lag CIGs (Rickett and Sava 2002) or time-lag CIGs (Sava and Fomel 2006), which can be transformed into angle gathers (Sava and Fomel 2003) for easier analysis especially in anisotropic media (Sava and Alkhalifah 2012; Alkhalifah and Fomel 2011). Alternatively, we can construct common-image-point gathers (CIPs), which are subsets of extended images constructed for all lags at fixed coordinates in the image. The points where we construct the gathers can be automatically identified using image features, e.g., reflectivity strength, spatial coherency, etc. (Cullison and Sava 2011) .

In anisotropic media, the extrapolation of the source and receiver wavefields needs to take anisotropy into account. This requires that we have access to proper anisotropic parameter description of the medium. For transversely isotropic (TI) media, this implies that we need to know the anisotropy model parameter η responsible for the anellipticity behaviour of the phase velocity. This parameter, together with the normal moveout (NMO) velocity described along the symmetry axis direction, enables us to perform accurate imaging in TI media (Alkhalifah, Fomel, and Biondi 2001). The axis of symmetry velocity v_{p_z} for a medium with a vertical symmetry axis is mainly responsible for placing reflections at their accurate depth positions. Thus, for anisotropic media, the key parameter for proper imaging and focusing is η. Ignoring η yields residual moveout in subsurface offsets and angle gathers (Alkhalifah and Fomel 2011), and it yields even more distinct features in extended images.

CIPs have been used for wavefield tomography (Yang and Sava 2010, 2011). This methodology builds on the well-established differential semblance optimization technique of Shen and Symes (2008) and Symes (2009). The essential feature of this method is that optimization minimizes an objective function defined based on the distortion of migrated images relative to an ideally focused image. The residual is formulated using a penalty function representing a perfectly focused image: the penalty is zero when the image is ideally focused and monotonically increases as a function of velocity error.

In this paper, we analyze the extended images in anisotropic media, specifically TI media, with the goal of establishing a baseline relative to which to define an objective function for wavefield tomography. The extended images provide image point extensions as a function of space and time lags. Embedded in these lag sections is valuable image focusing information, which can be used to analyze the model accuracy used in the wavefield extrapolation. As a result, we use such lag sections to characterize the response of the extended images to ignoring anisotropy in RTM. We find that the anisotropy error leaves a distinctive signature in migrated extended images. We restrict our attention to the analysis of migrated images in order to explore the specific information provided by such images for anisotropic wavefield tomography. The anisotropic tomography itself is a large topic that we leave outside the scope of this paper.

THEORY

Conventional wavefield-based imaging consists of two major steps: the wavefield reconstruction and the imaging condition (Berkhout 1982; Claerbout 1985). The major drivers for the accuracy of this technique are the source and receiver wavefields, which depend on space $\mathbf{x} = \{x, y, z\}$ and time t. Wavefield reconstruction in a tilted TI (TTI) anisotropic medium requires numeric solutions to a pseudo-acoustic wave equation (Alkhalifah 2000), e.g., the time-domain method of Fletcher, Du, and Fowler (2009) and Fowler, Du, and Fletcher (2010), which consists of solving a system of second-order coupled equations:

$$\frac{\partial^2 p}{\partial t^2} = v_{p_x}^2 H_2\left[p\right] + v_{p_z}^2 H_1\left[q\right], \tag{1}$$

$$\frac{\partial^2 q}{\partial t^2} = v_{p_n}^2 H_2\left[p\right] + v_{p_z}^2 H_1\left[q\right]. \tag{2}$$

Here, p and q are two wavefields dependent on space $\mathbf{x}$ and time t; H_1 and H_2 are differential operators applied to the quantity in the square brackets. Alternative formulations, e.g., that of Duveneck and Bakker (2011) and Zhang, Zhang, and Zhang (2011), provide expressions for stable extrapolation in more general cases, including TTI. The quantities v_{p_z}, v_{p_x}, and v_{p_n} are the parallel, perpendicular, and "NMO" velocities used to parametrize a generic TTI medium. If we describe the medium using the parameters introduced by Thomsen (2001), the velocities are related to the anisotropy parameters ϵ and δ by the relations $v_{p_n} = v_{p_z}\sqrt{1+2\delta}$ and $v_{p_x} = v_{p_z}\sqrt{1+2\epsilon}$. Thus, the quantities H_1 and H_2 depend on the medium parameters, as well as θ_a that describes the angle made by the TI symmetry axis with the vertical and ϕ_a the azimuth angle of the plane that contains the tilt.

A conventional imaging condition based on the reconstructed wavefields defines the image as the zero lag of

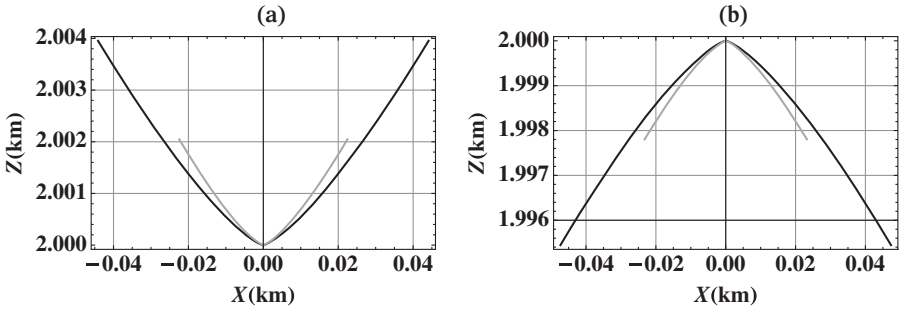


Figure 1 Image point defocusing corresponding to isotropic post-stack migration with the correct velocity of 2 km/s in an anisotropic medium with (a) $\eta = 0.1$ (grey curve), and $\eta = 0.2$ (black curve), and (b) $\eta = -0.1$ (grey curve) and $\eta = -0.2$ (black curve).

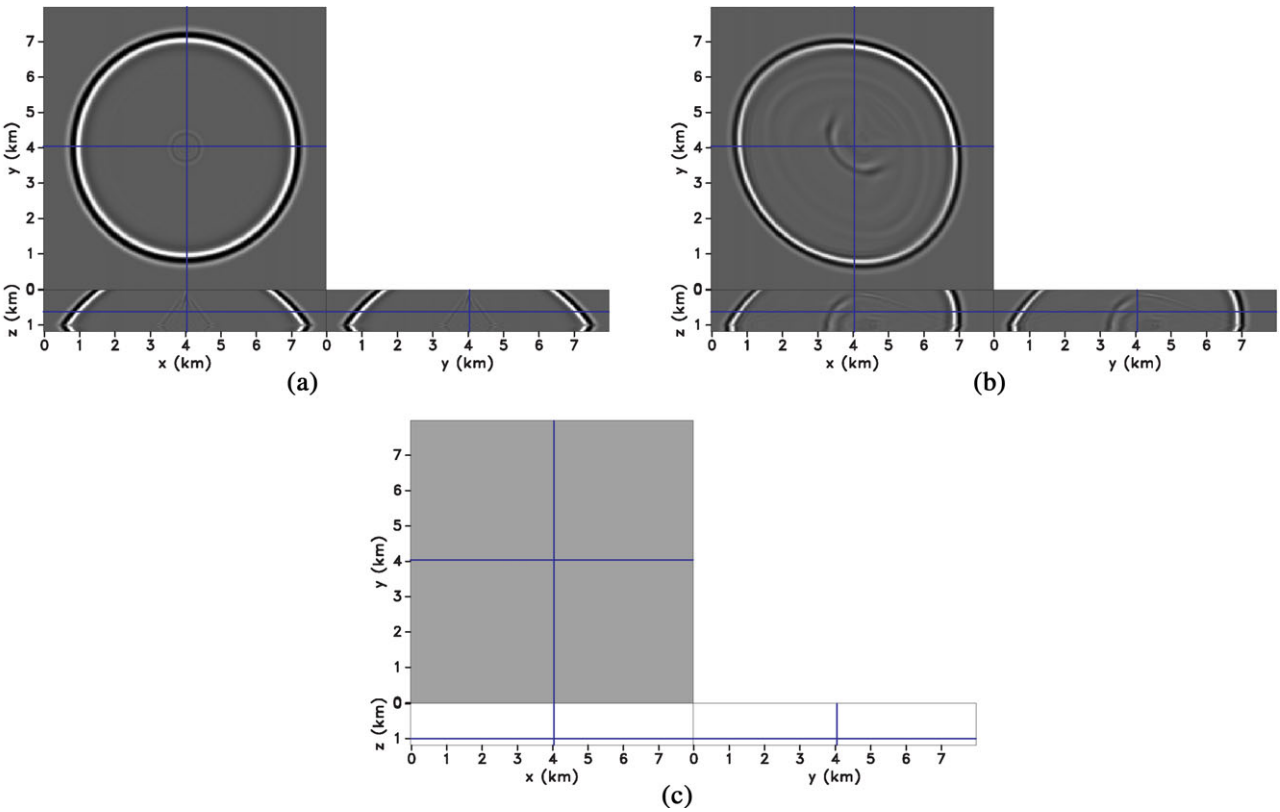


Figure 2 3D model used to illustrate wide-azimuth extended images in anisotropic media. Panels (a) and (b) show the wavefields corresponding to a single source at $\{x, y\} = \{4, 4\}$ km for VTI and TTI media, respectively. The model (c) consists of a horizontal reflector in constant velocity.

the cross-correlation between the source and receiver wavefields (Claerbout 1985). An extended imaging condition is a generalization of the conventional imaging condition in that it retains in the output image acquisition or illumination parameters. For example, we can generate image extensions by correlation of the wavefields shifted symmetrically in space (Rickett and Sava 2002; Sava and Fomel 2005) or in time (Sava and Fomel 2006). This separation is simply the lag of the cross-correlation between the source and receiver wavefields (Sava and Vasconcelos 2011)

$$R(\mathbf{x}, \boldsymbol{\lambda}, \tau) = \sum_{shots} \sum_{t} W_s(\mathbf{x} - \boldsymbol{\lambda}, t - \tau)\, W_r(\mathbf{x} + \boldsymbol{\lambda}, t + \tau)\,. \qquad (3)$$

Here R represents the migrated image that depends on position $\mathbf{x}$, and the quantities $\boldsymbol{\lambda}$ and τ are cross-correlation lags in space and time, respectively. The source and receiver

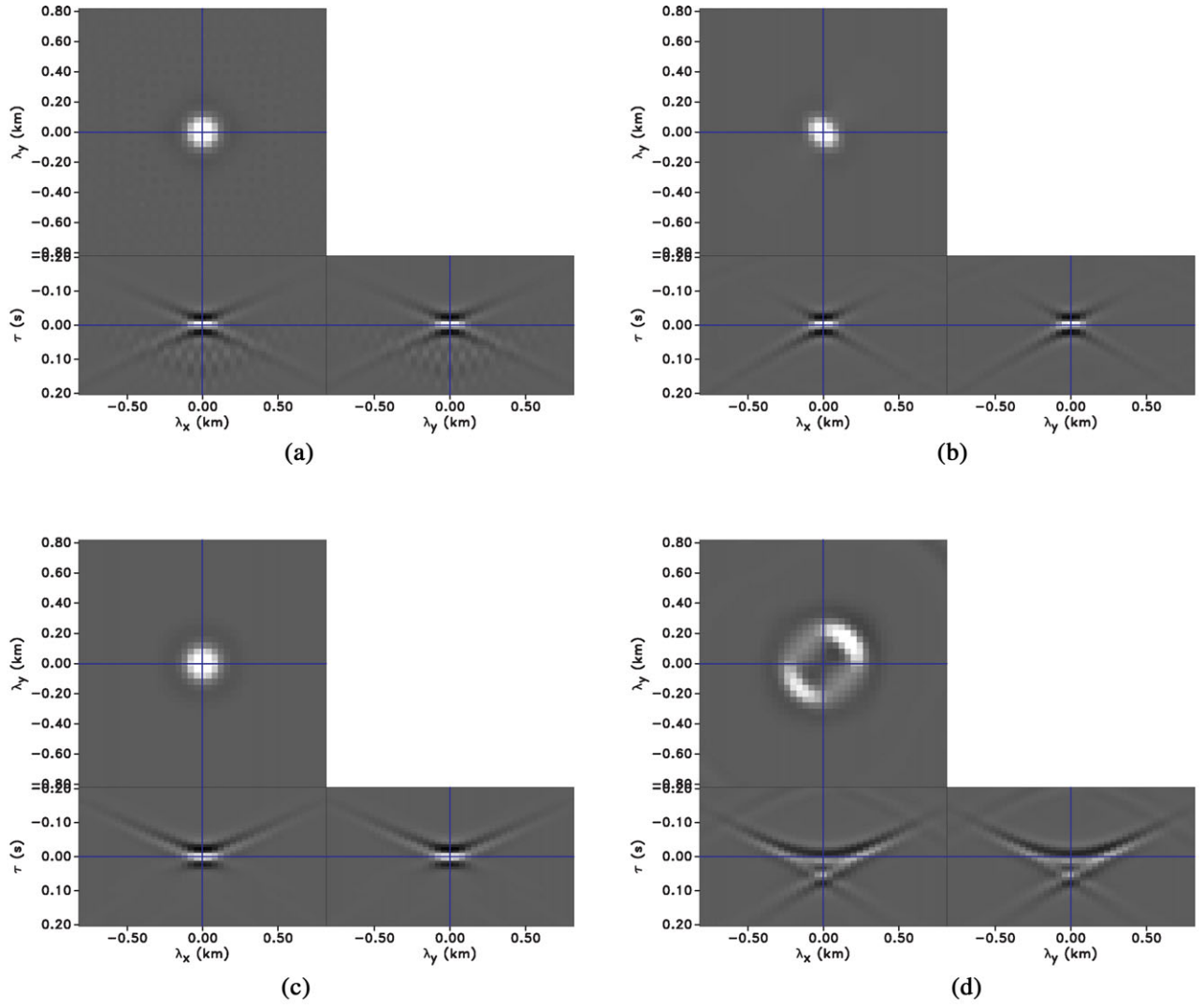


Figure 3 Extended CIPs at $\{x, y, z\} = \{4, 4, 1\}$ km for many sources distributed uniformly on the surface. The images are obtained by (a)–(b) anisotropic migration and (c)–(d) isotropic migration of the VTI data (left) and TTI data (right).

wavefields used for imaging, W_s and W_r, are the wavefields indicated by p in equations (1) and (2). The conventional imaging condition represents a special case of equation (3) for $\boldsymbol{\lambda} = \mathbf{0}$ and $\tau = 0$.

Various techniques have been proposed to convert the space- and time-lag extensions into reflection angles (Sava and Fomel 2003, 2006; Sava and Vlad 2011; Sava and Alkhalifah 2012) thus facilitating amplitude and velocity analysis in complex geologic structures. In this paper, we do not follow this route but instead concentrate on the interpretation of the moveout observed as a function of lags directly. A similar analysis can be done in the angle domain, but in this paper, we disregard this possibility.

As indicated earlier, CIPs constructed using a correct Earth model (and good subsurface illumination) reveal reflections as focused events at zero space and time lags. This shape has a straightforward physical interpretation. Following the discussion by Sava and Vlad (2011), the wavefield at a reflection point can be conceptually decomposed into planar components, each corresponding to a different propagation direction. We emphasize that we use the word "decomposition" only with a conceptual meaning and not a practical one. Other researchers have proposed actual decomposition of the wavefields into elementary planar components with different directions, but we do not follow that path because it is costlier and more difficult to implement in practice.

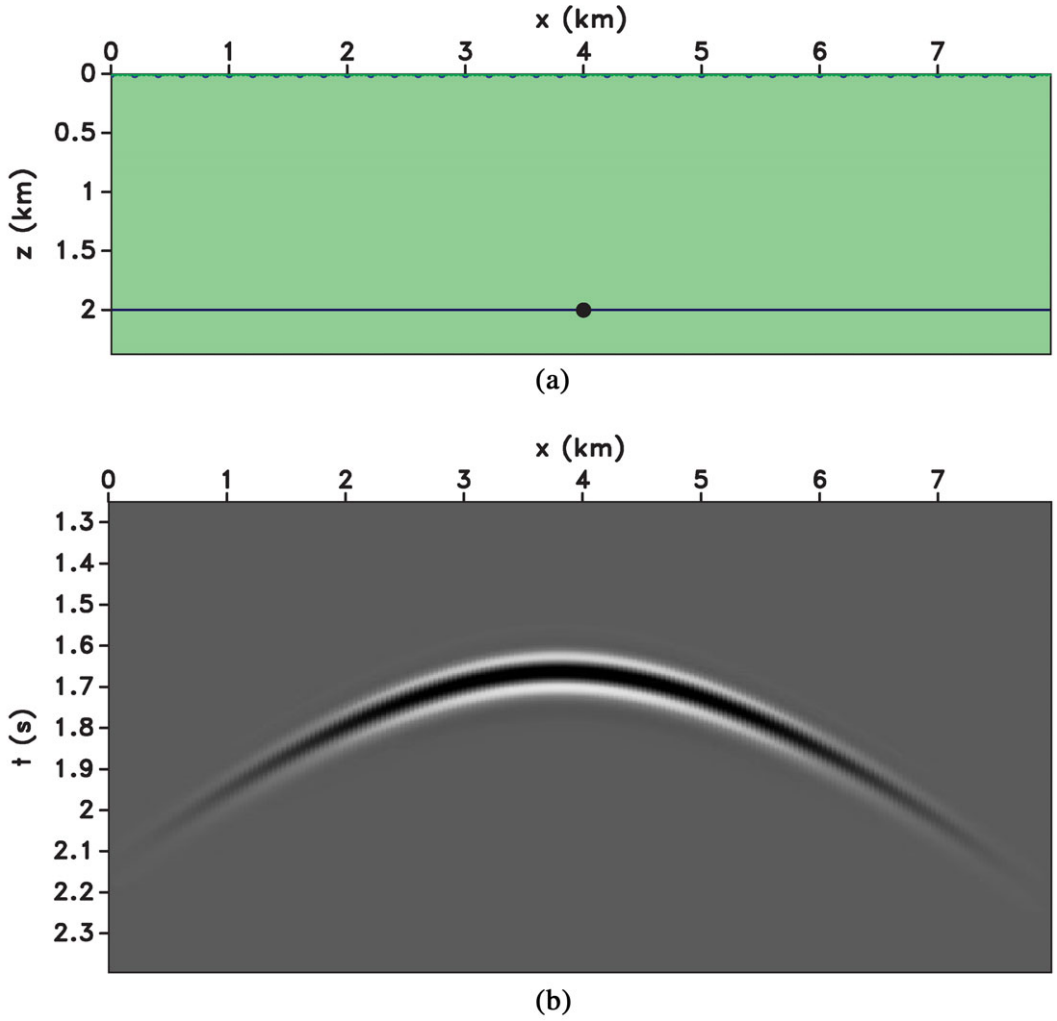


Figure 4 (a) 2D homogeneous model used to study the dependence of the extended CIPs with anisotropy, and (b) one shot gather for a source located at $\{x, z\} = \{3.4, 0\}$ km. The Earth model is anisotropic and characterized by parameter $\eta = 0.25$.

Nevertheless, the source and receiver wavefields at a reflection point where we construct a CIP gather behave as if they were strictly planar. Other planar components of the same non-planar wavefield exist, but they are located elsewhere in space and thus do not contribute to the CIP under consideration. By simultaneously shifting the source and receiver wavefields in space and time, we obtain non-zero images only when the space and time lags are related to one another by a relation that depends on the 3D angles of incidence and local material properties (Sava and Vlad 2011). It turns out that each direction of illumination is described in a CIP by a planar event in the $\boldsymbol{\lambda} - \tau$ space. This observation is true both for isotropic and anisotropic media, but the physical interpretation is different: in isotropic media, the planar events identify directions corresponding to group angles, whereas in anisotropic media, the planar events identify directions corresponding to phase angles (Sava and Alkhalifah 2012).

The most relevant property for velocity model building is that the planar events corresponding to different illumination directions overlap at zero space and time lags, i.e., at the origin of the extended space of each CIP. This is simply because we choose, by construction, points on reflectors, so ideally, we form an image at zero lag from all propagation directions at the same place on the reflector. This is just a restatement of the semblance principle that says that the imaged geologic structure does not depend on the direction of illumination, assuming that the model used for wavefield reconstruction is correct. If the reconstruction is incorrect, then not all planar events in a CIP go through zero lag in space

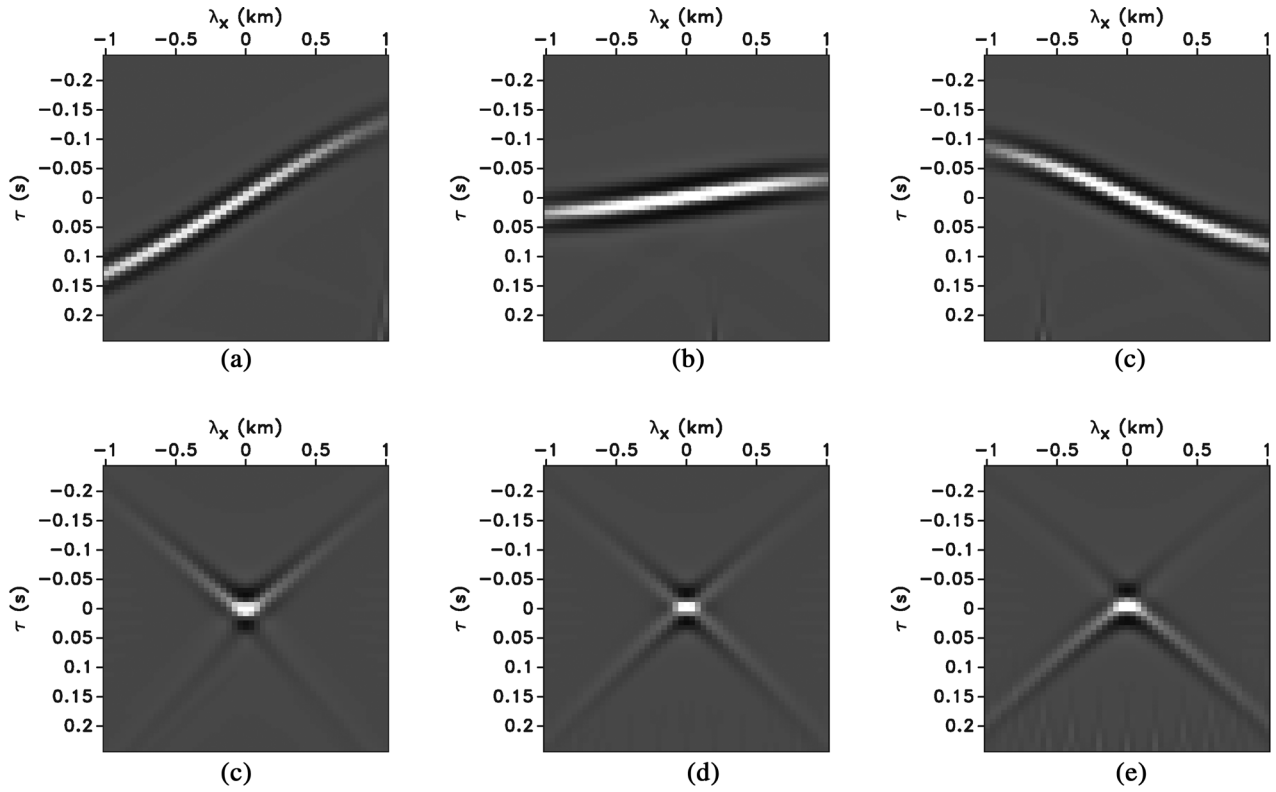


Figure 5 2D extended CIPs at $\{x, z\} = \{4, 0\}$ km for the constant model, (Fig. 4(a)). The extended images (a)–(c) correspond to individual shots at surface coordinates $x = \{3.2, 4.0, 4.8\}$ km and are obtained from wavefields reconstructed with the correct $\eta = 0.25$. The extended images (d)–(f) correspond to anisotropy characterized by parameter $\eta = \{0.15, 0.25, 0.35\}$.

and time, thus indicating that not all illumination directions produce the image at the same depth. This information can be used for velocity analysis.

In anisotropic media, wavefield reconstruction depends on more than one parameter. For TI media, one simple way to describe the model parameters is through velocity v and the anisotropic parameter η. Reconstructed wavefields can be inaccurate due to inaccuracies in both parameters; therefore, the effects observed in extended CIPs are simultaneously due to both. As for other domains, it is not trivial to differentiate between the effects of velocity and anisotropy error on the model. It is, nevertheless, interesting to understand how each parameter controls the observed moveout, which is a prerequisite for tomography. Thus, we concentrate on the moveout due to anisotropy, assuming that the velocity has already been updated using other conventional methods. This is natural since the common velocity model building procedure starts with an isotropic assumption of the Earth.

Alkhalifah and Fomel (2011) show using anisotropic parameter continuation that the residual anisotropic response for post-stack imaging in homogeneous media, specifically residuals corresponding to the anisotropy parameter η, has a "V"-like shape. This response stems from the fourth-order nature of the η influence on travel time as a function of offset. A residual reconstruction of such travel time maps the fourth-order influence to a "V"-shaped (rather than a residual hyperbolic) moveout as shown in Fig. 1. The slope of the "V" depends on the value of η, where negative η provides a flipped "V" signature. We will later see a similar response for the pre-stack case even in complex media.

The V-shaped signature in the extended images exists regardless of the complexity of the background isotropic (or elliptically anisotropic) velocity model. Thus, such a behaviour also characterizes the extended images for pre-stack data in complex anisotropic media. This is because the major wavefield complexities are compensated during the

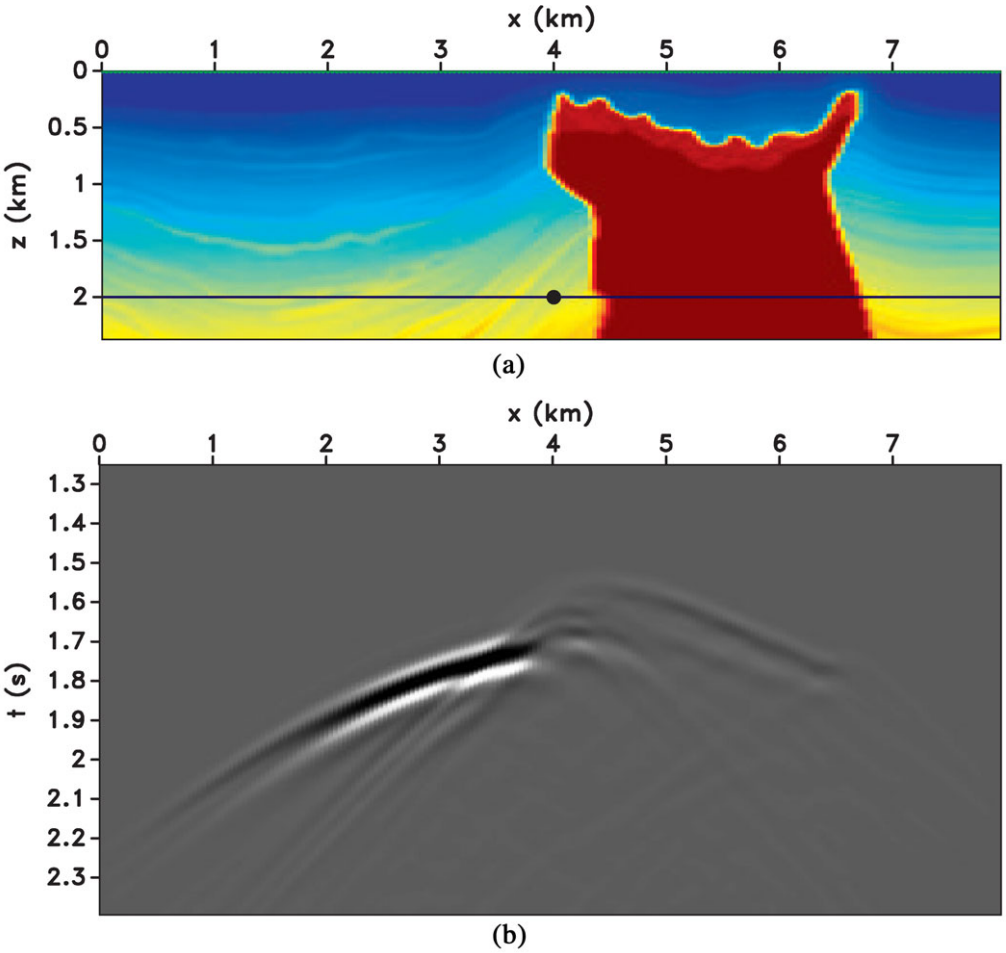


Figure 6 (a) 2D salt model used to study the dependence of the extended CIPs with anisotropy and (b) one shot gather for a source located at $\{x, z\} = \{3.4, 0\}$ km. The Earth model is anisotropic and characterized by parameter $\eta = 0.25$.

wavefield reconstruction in anisotropic media. Most of what remains is the influence of anisotropy that resembles the established behaviour of post-stack depth images. This property could be used to separate the effects of anisotropy from those of velocity, with applications to anisotropic Earth model building.

EXAMPLES

The model for our first example (Fig. 2(c)) consists of a horizontal reflector in a 3D constant velocity model. Figure 2(a) and (b) depicts one snapshot of the wavefields for a source located on the surface in TI with vertical symmetry axis (VTI) and TTI models, respectively. The models are characterized by the parameters $\epsilon = 0.30$ and $\delta = -0.10$ and, for the TTI model, by $\theta_a = 35^\circ$ and $\phi_a = 45^\circ$. Figure 3(a) and (b) depicts extended CIPs at $(x, y, z) = (4, 4, 1)$ km for many sources distributed uniformly on the surface and correct Earth models. All CIPs show focusing at zero lags in space and time, thus indicating wavefield reconstruction with a correct Earth model. However, the CIPs constructed with isotropic migration (Fig. 3(c) and (d)) are not focused, thus indicating that the CIPs are sensitive to anisotropy inaccuracy.

The next examples illustrate the behaviour of the extended images as a function of anisotropy inaccuracy in homogeneous and laterally heterogeneous models, respectively. The models are shown in Figs. 4(a) and 6(a). The data, exemplified in Figs. 4(b) and 6(b) are constructed with anisotropy characterized by parameter $\eta = 0.25$. Figure 7(a)–(c) shows the extended images for different shot locations obtained by RTM with the correct salt model. The figures indicate dependence of the CIPs with the angle of illumination, which can

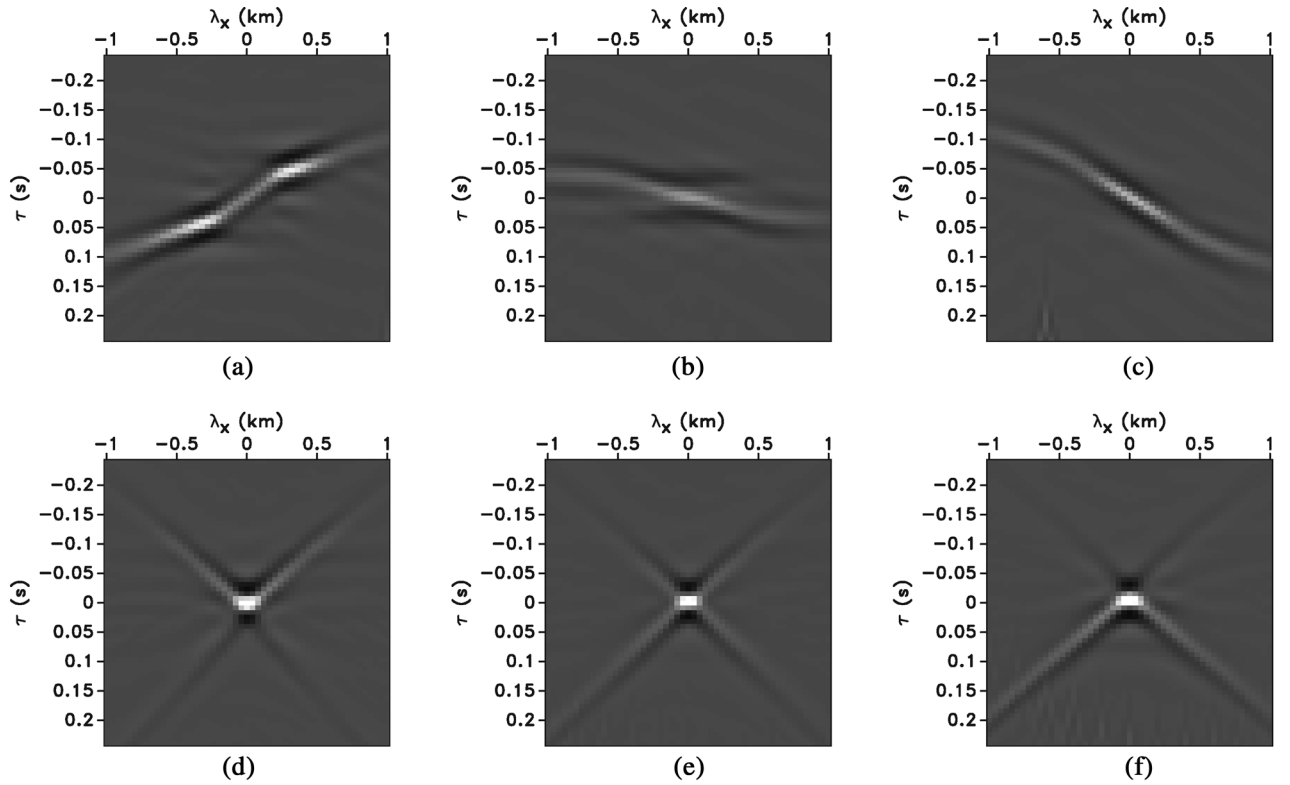


Figure 7 2D extended CIPs at $\{x, z\} = \{4, 0\}$ km for the salt model, (Fig. 6(a)). The extended images (a)–(c) correspond to individual shots at surface coordinates $x = \{3.2, 4.0, 4.8\}$ km and are obtained from wavefields reconstructed with the correct $\eta = 0.25$. The extended images (d)–(f) correspond to anisotropy characterized by parameter $\eta = \{0.15, 0.25, 0.35\}$.

be exploited for angle decomposition. The summation for all shots leads to the CIP shown in Fig. 7(e), which shows focusing of the image at zero space and time lags. This is due to the fact that all shots leave an imprint on the CIPs at zero space and time lags, but at different slopes that depend on the illumination angle, Fig. 7(a)–(c).

For incorrect η, the resulting response has an overall "V" shape similar to that seen for residual post-stack migration. The slope of the "V" flanks, as illustrated in Fig. 7(d)–7(f) depends on η. For η close to the correct value, the "V" energy tends to approach the apex, and for correct η, it focuses at its apex (Fig. 7(e)). This general behaviour is consistent regardless of the complexity of the medium, especially with respect to the portion of the signature that is near the apex. For comparison, Fig. 5(d)–(e) shows extended gathers corresponding to the same values of η as in Fig. 7(d)–(e). Despite the fact that the background velocity model is significantly different, i.e., constant versus salt, the CIPs are comparable, thus indicating that they are mainly influenced by the anisotropy parameters. Of course, for a varying η, such signatures reflect an effective value under the effective medium theory. This property can be exploited for anisotropic migration velocity analysis.

Finally, Fig. 8(a) and 8(b) illustrates the behaviour of 3D anisotropic extended CIPs for a North Sea field data set. Figure 8(a) shows the velocity model, and Figure 8(b) shows the corresponding conventional image. Although the Earth is known to be anisotropic in this region, the image shown in Fig. 8(b) uses isotropic migration, and thus is partially inaccurate.

Figure 9 shows the same image as the one shown in Fig. 8(b) but in a perspective view and with three slices selected at a fixed inline, crossline, and depth, respectively. Overlain on the figure are also the locations of the CIPs constructed to analyze the accuracy of the image. CIPs are indicated by small ellipsoids instead of points (Cullison and Sava 2011). The flat ellipsoids represent the structure tensor constructed at each point, and the orientation of the ellipsoids in 3D space indicates the orientation of the reflectors at each position. We construct extended CIPs at each of these 5000 locations, which represents an enormous cost reduction relative to CIGs constructed for all depths at many regularly spaced positions on the surface.

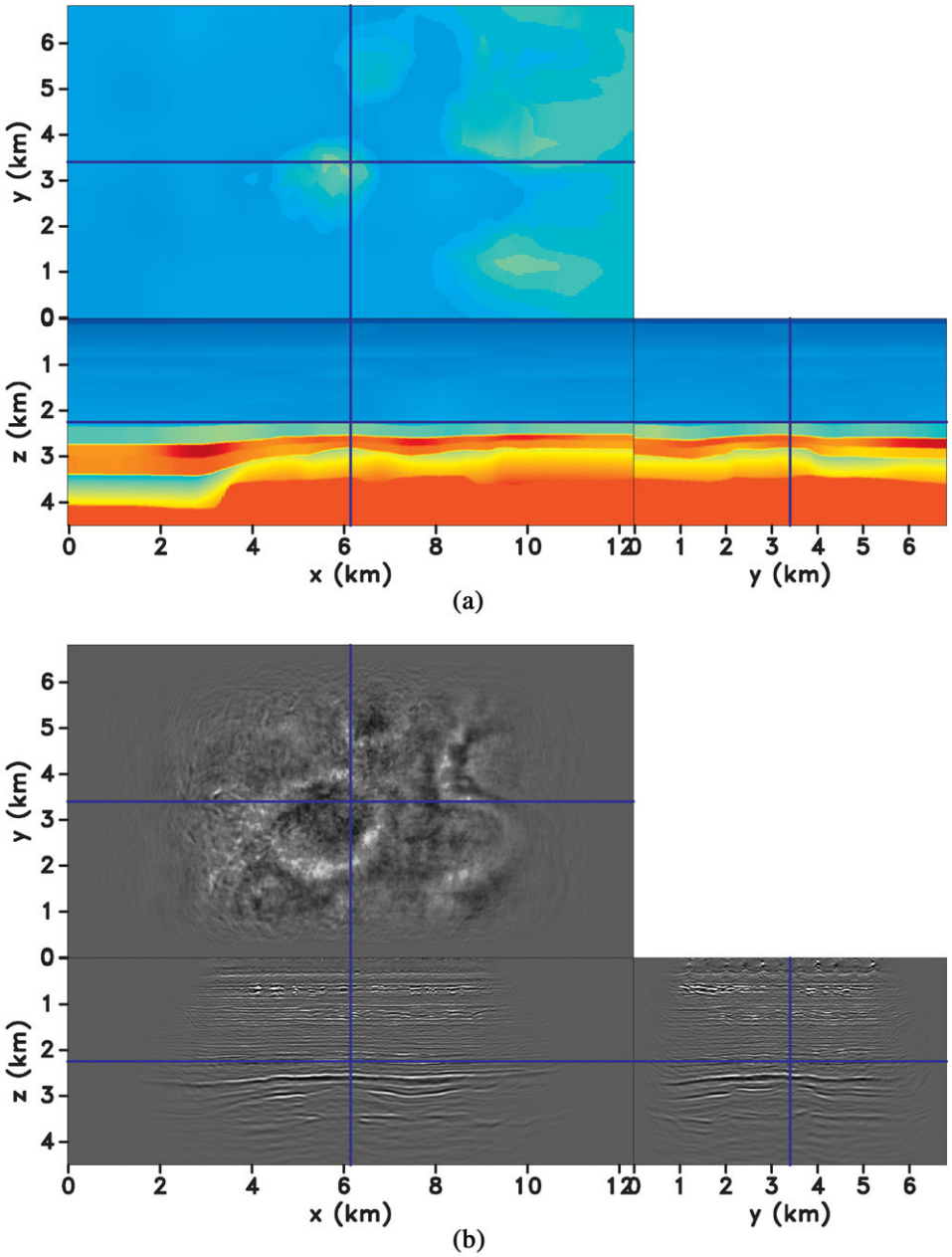


Figure 8 North Sea model: (a) P-wave velocity and (b) isotropic image.

Figures 10 and 11 depict different locations in the image, corresponding to CIPs automatically generated using the method discussed earlier. In Fig. 10, the CIP is selected in the middle of the image; therefore, the inline illumination is good, although the cross line aperture is more limited. In the inline direction, we observe the characteristic V, indicating that the model currently used for imaging is actually accurate, but the anisotropy is not accurate. The inline behaviour should, in principle, repeat in the crossline direction, although this is not what happens in this case due to the limited aperture. Partial illumination is also visible in Fig. 11. In this case, we see a CIP located at the edge of the model, where the illumination is mainly from one side even in the inline direction.

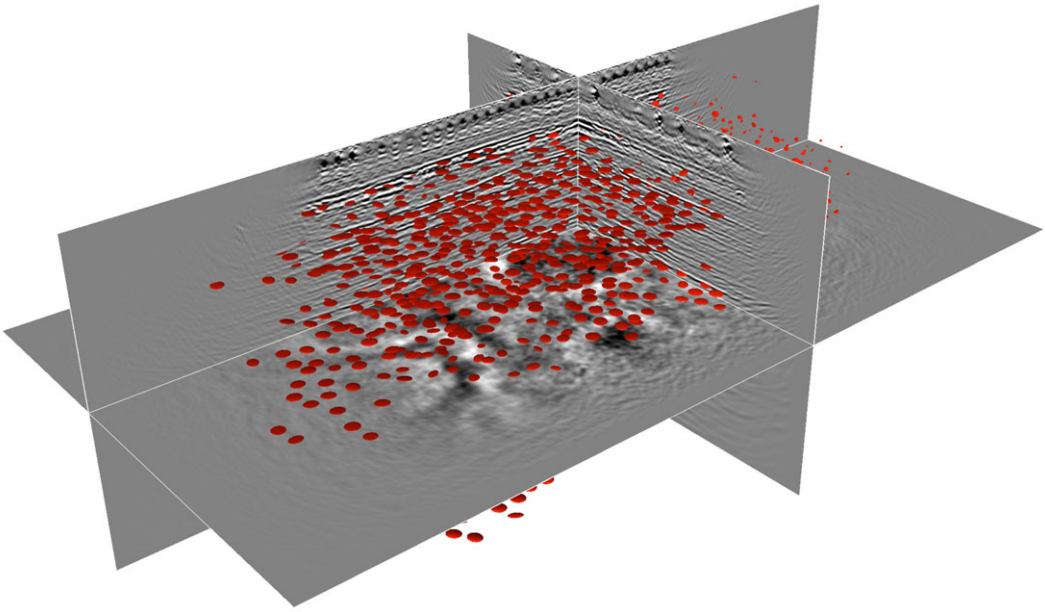


Figure 9 Image with the picked locations of the CIP gathers. The ellipsoids indicate the local slope and azimuth of the geologic structure.

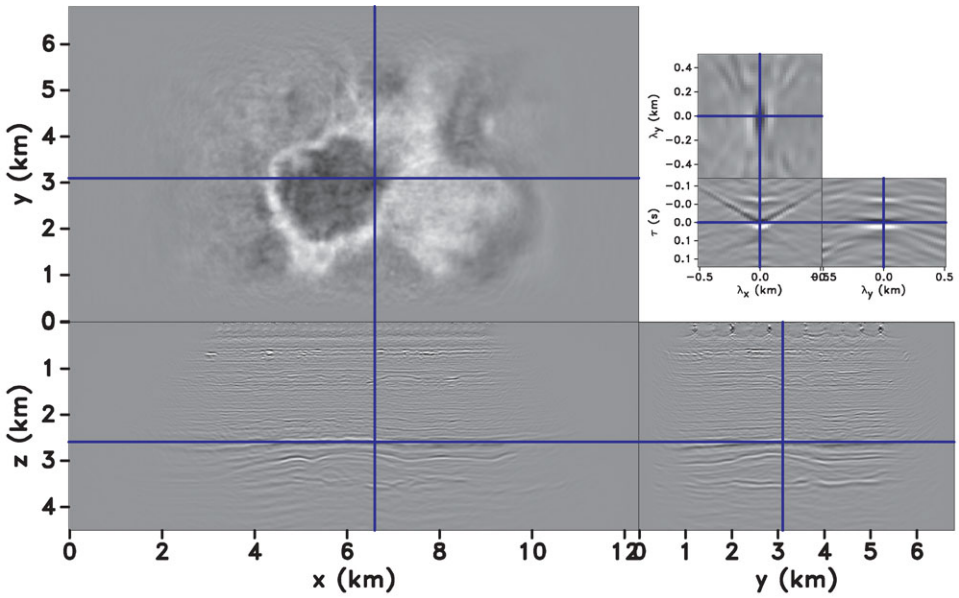


Figure 10 Conventional image with inset indicating the extended image at location "A" indicated by the intersecting lines.

DISCUSSION

Despite the relative complexity of a particular model, ignoring anisotropy in the extrapolation of the wavefield yields a distinct signature in extended images that is different than those observed for an inaccurate velocity model. The shape of this distinct signature generally survives even if the wavefield has passed through salt bodies. For negative η in the medium, which is rare, the V shape resulting from ignoring anisotropy is flipped, with a behaviour that is similar to the positive η.

A natural progression in velocity model building in complex media is to assume initially that the medium is isotropic as we find the velocity model that produces the best focusing at zero lag. At a certain stage, the velocity update process based on the second-order nature of the residual moveout ceases to update the velocity model as residuals are described

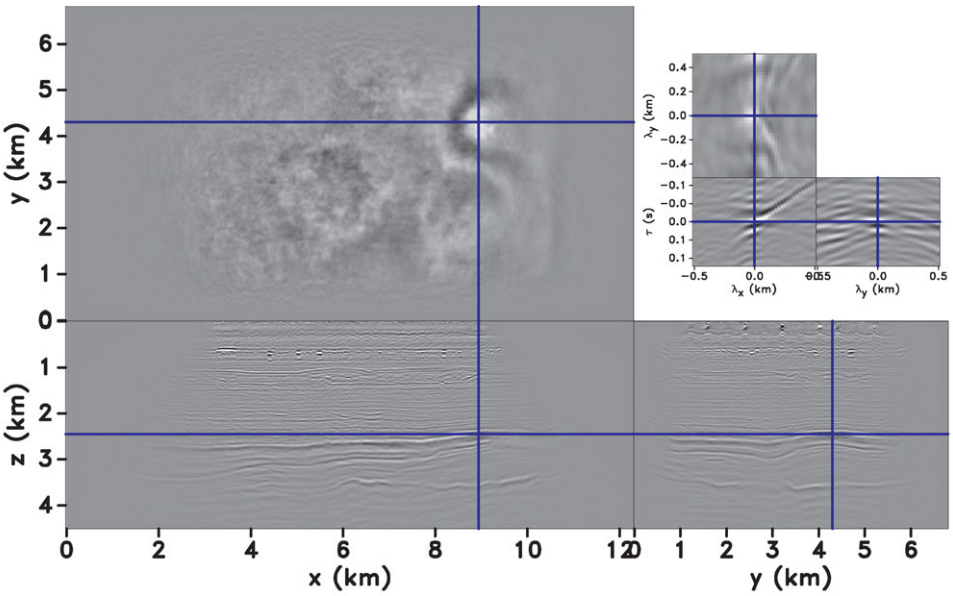


Figure 11 Conventional image with inset indicating the extended image at location "B" indicated by the intersecting lines.

by higher order functions. This is exactly the case for the real data example shown earlier, in which case the isotropic velocity model fails to suppress the V-shaped signature observed in the extended images. Extrapolating the focusing residual using an operator that updates the η field accordingly is left outside the scope of this paper.

CONCLUSIONS

The distinct anisotropic signatures, needed for parameter estimation, tend to get lost in the mist of the complexity of the velocity in the medium. Extended images preserve such signatures, which allows for direct anisotropy analysis. The slope of the residual moveout in extended CIPs mainly depends on η, which simplifies parameter estimation in anisotropic media. A comparison of extended images between simple and complex models supports our assertion.

ACKNOWLEDGEMENTS

This work was supported in part by the Center for Wave Phenomena at Colorado School of Mines and by the King Abdullah City for Science and Technology (KACST). The authors would like to thank Statoil ASA and the Volve licence partners, ExxonMobil E&P Norway, and Bayerngas Norge for the release of the Volve data. The reproducible numeric examples in this paper use the Madagascar open-source software package freely available from http://www.ahay.org.

REFERENCES

Alkhalifah T. 2000. An acoustic wave equation for anisotropic media. *Geophysics* **65**, 1239–1250.

Alkhalifah T. and Fomel S. 2011. The basic components of residual migration in VTI media using anisotropy continuation. *Journal of Petroleum Exploration and Production Technology* **1**, 17–22.

Alkhalifah T., Fomel S. and Biondi B. 2001. The space-time domain: theory and modelling for anisotropic media. *Geophysical Journal International* **144**, 105–113.

Baysal E., Kosloff D. D. and Sherwood J. W. C. 1983. Reverse time migration. *Geophysics* **48**, 1514–1524.

Berkhout A. J. 1982. *Imaging of Acouting Energy by Wave Field Extrapolation*. Elsevier.

Clærbout J. F. 1985. *Imaging the Earth's Interior*. Blackwell Scientific Publications.

Cullison T. and Sava P. 2011. An image-guided method for automatically picking common-image-point gathers. 81st SEG annual international meeting, San Antonio,USA, Expanded Abstracts.

Duveneck E. and Bakker P. M. 2011. Stable P-wave modeling for reverse-time migration in tilted TI media. *Geophysics* **76**, S65–S75.

Fletcher R. P., Du X. and Fowler P.J. 2009. Reverse time migration in tilted transversely isotropic (TTI) media. *Geophysics* **74**, WCA179–WCA187.

Fowler P. J., Du X. and Fletcher R. P. 2010. Coupled equations for reverse time migration in transversely isotropic media. *Geophysics* **75**, S11–S22.

Gray S. H., Etgen J., Dellinger J. and Whitmore D. 2001. Seismic migration problems and solutions. *Geophysics* **66**, 1622–1640.

McMechan G. A. 1983. Migration by extrapolation of time-dependent boundary values. *Geophysical Prospecting* **31**, 413–420.

Rickett J. and Sava P. 2002. Offset and angle-domain common image-point gathers for shot-profile migration. *Geophysics* **67**, 883–889.

Sava P. and Alkhalifah T. 2012. Wide-azimuth angle gathers for anisotropic wave-equation migration. *Geophysical Prospecting* **61**, 75–91.

Sava P. and Fomel S. 2003. Angle-domain common image gathers by wavefield continuation methods. *Geophysics* **68**, 1065–1074.

Sava P. and Fomel S. 2005. Coordinate-independent angle-gathers for wave equation migration. 75th SEG annual international meeting, Houston, USA Expanded Abstracts, 2052–2055.

Sava P. and Fomel S. 2006. Time-shift imaging condition in seismic migration. *Geophysics* **71**, S209–S217.

Sava, P. and Vasconcelos I. 2011. Extended imaging condition for wave-equation migration. *Geophysical Prospecting* **59**, 35–55.

Sava P. and Vlad I. 2011. Wide-azimuth angle gathers for wave-equation migration. *Geophysics* **76** S131–S141.

Shen P. and Symes W. W. 2008. Automatic velocity analysis via shot profile migration. *Geophysics* **73**, VE49–VE59.

Symes W. 2009. Migration velocity analysis and waveform inversion. *Geophysical Prospecting* **56**, 765–790.

Thomsen L. 2001. Seismic anisotropy. *Geophysics* **66**, 40–41.

Yang T. and Sava P. 2010, Wave-equation migration velocity analysis with extended common image-point gathers. 80th SEG annual international meeting, Denver, USA, Expanded Abstracts.

Yang T. and Sava P. 2011. Image-domain waveform tomography with two-way wave-equation. 81st SEG annual international meeting, San Antonio, USA, Expanded Abstracts.

Zhang Y., Zhang H. and Zhang G. 2011. A stable TTI reverse time migration and its implementation. *Geophysics* **76**, WA3–WA11.